

Performance Bounds for Velocity Estimation with Large Antenna Arrays

Caterina Giovannetti, *Graduate Student Member, IEEE*, Nicolò Decarli, *Member, IEEE*, and Davide Dardari, *Senior Member, IEEE*

Abstract—Joint communication and sensing (JCS) is envisioned as an enabler of future 6G networks. One of the key features of these networks will be the use of extremely large aperture arrays (ELAAs) and high operating frequencies, which will result in significant near-field propagation effects. This unique property can be harnessed to improve sensing capabilities. In this paper, we focus on velocity sensing, as using ELAAs allows the estimation of not just the radial component but also the transverse component. We derive analytical performance bounds for both velocity components, demonstrating how they are affected by the different system parameters and geometries. These insights offer a foundational understanding of how near-field effects play in velocity sensing differently from the far field and from position estimate.

Index Terms—Velocity estimation, Doppler, Near field radar, Extremely large aperture arrays (ELAAs), Cramér-Rao lower bound (CRLB), Joint communication and sensing (JCS)

I. INTRODUCTION

JOINT communication and sensing (JCS) is a technology that combines wireless data communication with radar sensing into a single system. Instead of using separate hardware and spectrum for each function, JCS enables devices to communicate and sense at the same time, often using the same signals and frequency bands. This integration improves spectrum efficiency, reduces hardware costs, opens up new applications, and it has been identified as a pillar for the forthcoming 6G [1]. Among the quantities that can be sensed concerning a passive target, Doppler-based velocity estimation relies on the principle that the frequency of a propagating wave changes when the target and the observer are in motion relative to each other [2]. By analyzing the frequency variations, radar systems can determine whether a target is approaching or receding and at what speed. However, only the radial velocity, i.e., the projection of the target velocity along the target-receiver direction, can produce frequency variations under traditional far-field operating conditions [2].

Recently, communication systems are shifting towards the adoption of extremely large aperture arrays (ELAAs) and high carrier frequencies, making traditional far-field assumptions for propagation no longer fulfilled [3]. In the last years, this operating condition has been deeply investigated for what concerns communication and localization [4], [5]. In the field of radar sensing, studies are still at the early stage and usually focus on the enhanced resolution offered in terms of

distance/angle estimation [6]–[8]. When dispersed antennas are employed, the ability to observe targets from different directions permits the estimation of the different velocity components using multi-static radars [9]. However, thanks to the adoption of ELAAs, this capability holds even for non-dispersed antennas, allowing to estimate not only the radial component of the velocity but also the transverse one. This is the concept of *velocity sensing* recently introduced in [10] when employing antenna arrays working in near-field conditions, enabling to get a full picture of the target velocity and trajectory using a monostatic radar instead of multi-static radars that require challenging synchronization and expensive hardware [7]. Such a capability makes large antenna arrays attractive for velocity estimation, in addition to the already-known benefits of near-field operations, such as improved spatial multiplexing even in line-of-sight (LOS) conditions [4], [11], the possibility of single-anchor localization [12] and high-resolution sensing [4], [13]. To the authors' knowledge, no studies are present investigating the theoretical performance limits for velocity estimation using large arrays in the near-field. The paper [10] studies a maximum likelihood velocity estimator and its adoption for predictive beamforming applications, but it does not analyze the performance bounds and how the different system and geometrical parameters affect the estimation capability.

In this paper, we analytically derive the performance bounds for velocity estimation using large arrays. Specifically, we show novel results according to which (i) the transverse velocity accuracy decreases quadratically with the target-receiver distance and (ii) for half-wavelength spaced arrays, it does not depend on the carrier frequency. This behavior is thus completely different from that of radial velocity estimation usually considered. Moreover, we depict the impact of the different system and geometrical parameters, highlighting the differences between near-field distance estimation and transverse velocity estimation using large arrays.

II. SIGNAL AND SYSTEM MODEL

We consider sensing of a passive point target in a 2D scenario using a single input multiple output (SIMO) monostatic radar at the base station (BS), thus with a single transmitting antenna and K receiving elements arranged according to a linear ELAA deployment. Denote with δ the antenna spacing and let us assume K to be odd. The reference system is placed with the origin corresponding to the central element of the ELAA at the BS, which is oriented along the x -axis (see Fig. 1). Denote with $\tilde{\mathbf{p}}_k = [x_k, y_k]^T$ the position of the k -th receiving antenna at the BS, for $k = -(K-1)/2, \dots, (K-1)/2$, so that $x_k = k\delta$, $y_k = 0$, $\forall k$, and $x_0 = 0$ represents the

C. Giovannetti and N. Decarli are with the National Research Council (CNR-IEIIT), and WiLab-CNIT, Bologna (BO), Italy (e-mail: {caterina.giovannetti, nicolo.decarli}@ieiit.cnr.it). C. Giovannetti is also with DEI, University of Bologna, Bologna (BO), Italy.

D. Dardari is with the Dipartimento di Ingegneria dell'Energia Elettrica e dell'Informazione "Guglielmo Marconi" (DEI), University of Bologna, and WiLab-CNIT, Bologna (BO), Italy, e-mail: davide.dardari@unibo.it.

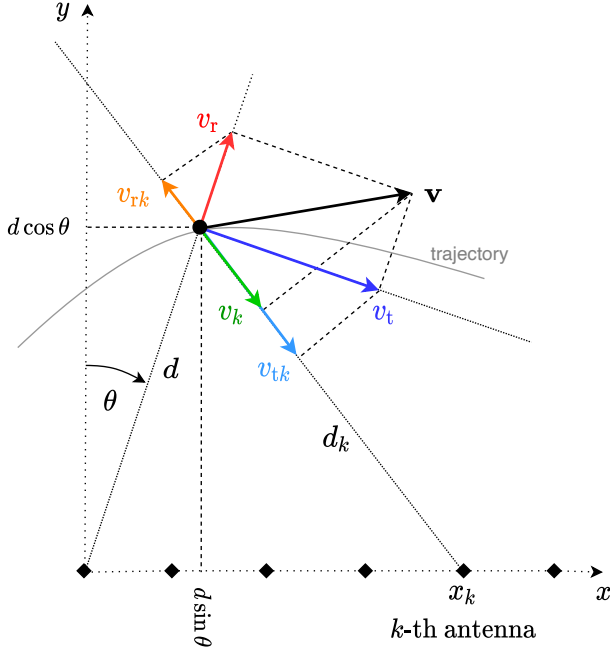


Fig. 1. Geometry of the scenario for velocity estimation with an ELAA.

array center. We assume a point target placed in position $\tilde{\mathbf{p}} = [d \sin \theta, d \cos \theta]^\top$ moving with velocity $\mathbf{v} = [v_r, v_t]^\top$ tangent to its trajectory on the plane, where v_r and v_t are the radial and transverse velocity components, respectively, with respect to the center of the ELAA (see Fig. 1). Let us now consider, for convenience, a polar coordinate system. In this case, we can write the target position as $\mathbf{p} = [d, \theta]^\top$, where $d = \|\tilde{\mathbf{p}}\|$ denotes the distance between the target and the central element of the receiving ELAA at the BS, and θ denotes the angle with respect to the boresight direction of the receiving ELAA (i.e., the angle of arrival (AoA) of the signal received at the BS). Define d_k the distance between the target and the k -th receiving antenna that can be expressed as

$$d_k = \|\tilde{\mathbf{p}} - \tilde{\mathbf{p}}_k\| = d \sqrt{1 + \frac{x_k^2}{d^2} - \frac{2x_k \sin \theta}{d}}. \quad (1)$$

The central antenna element of the BS transmits the signal $s_m(t)$ modulated at the carrier frequency f_c , that is

$$\tilde{s}(t) = \Re \left\{ \sum_m s_m(t) e^{j2\pi f_c t} \right\} \quad (2)$$

where the baseband signal $s_m(t)$ is realized as an orthogonal frequency-division multiplexing (OFDM) transmission spanning N subcarriers and M OFDM symbols. In particular, the m -th symbol component is given by

$$s_m(t) = \sum_n \sqrt{P} u_{m,n} e^{j2\pi n \Delta f t} \text{rect} \left(\frac{t - mT_{\text{sym}}}{T_{\text{sym}}} \right) \quad (3)$$

where $P = P_T/N$ is the power allocated to each subcarrier, P_T is the total transmit power, and $u_{m,n}$ is the data symbol transmitted in the m -th OFDM symbol and n -th subcarrier, with $\mathbb{E}\{|u_{m,n}|^2\} = 1$, for $m = -(M-1)/2, \dots, (M-1)/2$ and $n = -(N-1)/2, \dots, (N-1)/2$. We denote with $\mathbb{E}\{\cdot\}$

the statistical expectation. The symbol time is $T_{\text{sym}} = T + T_{\text{cp}}$ where T_{cp} stands for the cyclic prefix duration and $T = 1/\Delta f$, with Δf indicating the subcarrier spacing (SCS).

After classical cyclic prefix removal and FFT processing, the received signal is

$$\begin{aligned} r_{m,n,k} &= y_{m,n,k} + z_{m,n,k} \\ &= \sqrt{P} \beta_{m,n,k} u_{m,n} e^{-j2\pi f_n \tau_k} e^{j2\pi \nu_{n,k} m T_{\text{sym}}} + z_{m,n,k} \end{aligned} \quad (4)$$

where $f_n \triangleq f_c + n\Delta f$ is the frequency associated with the n -th subcarrier, $\beta_{m,n,k}$ is the channel gain coefficient, $\tau_k = \frac{d+d_k}{c}$ is the round-trip delay associated to the k -th receiving antenna, and $\nu_{n,k} = \frac{f_n}{c} (\mathbf{v}_r + \mathbf{v} \cdot \mathbf{e}_k)$ is the round-trip Doppler shift, with $\mathbf{a} \cdot \mathbf{b}$ indicating the scalar product between vectors \mathbf{a} and \mathbf{b} , and c the speed of light. Here, the term $\mathbf{e}_k = \mathbf{d}_k / \|\mathbf{d}_k\|$ is a unit norm vector denoting the direction between the k -th receiving antenna element and the target, so that $\nu_{n,k}$ includes a component which is the projection of the target's velocity along this direction for each receiving antenna. The term $z_{m,n,k}$ indicates the additive white Gaussian noise (AWGN), with $z_{m,n,k} \sim \mathcal{CN}(0, \sigma^2)$ and $\sigma^2 = k_B T_0 F \Delta f$, being k_B the Boltzmann constant, T_0 the reference temperature, and F the receiver noise figure. We consider the channel gain equal for all the antennas, which is reasonable for the practical size of the receiving ELAA and small relative bandwidth $B = N\Delta f \ll f_c$, so that we can write $\beta_{m,n,k} = \beta, \forall m, n, k$.

Starting from the received signal (4), the BS aims at estimating the position \mathbf{p} and velocity \mathbf{v} through the estimation of their components $[d, \theta]$ and $[v_r, v_t]$, respectively, thanks to the use of the ELAA.

III. VELOCITY ESTIMATION PERFORMANCE BOUNDS

The optimal way of processing the receiving signal would require the joint estimation of all the unknown parameters $\Theta = \{d, \theta, v_r, v_t\}$ from the $M \times N \times K$ observations. This would imply a very high complexity, especially when operating in the near-field region where the planar wavefront approximation does not hold. To focus here on the estimation of the radial and transverse velocity components when adopting the ELAA, we assume that the distance d and the AoA θ have already been estimated, as done also in [10]. This can be realized by exploiting the information coming from the different subcarriers (e.g., for distance estimation), and/or from the phase profile along the array caused by the spherical wavefront (e.g., for distance and angle estimation) [8]. Thus, starting from this assumption, we want to evaluate the performance limits on the estimation mean square error (MSE) of the radial and transverse velocity components v_r and v_t . Since the transmitted symbols are known by the receiver and used as pilots, in the following we consider $u_{m,n} = 1$ in (4); moreover, τ_k is known since the distance d and the angle θ have been assumed already estimated.

The velocity estimation quality in terms of MSE is lower bounded by the Cramér-Rao Lower Bound (CRLB) [14]. In this case, we have two scalar parameters to consider for the

CRLB analysis, that are $\Theta = \{v_r, v_t\}$. The (i, j) -th element of the Fisher information matrix (FIM) can be obtained as [14]

$$[\mathbf{J}]_{i,j} = \frac{2}{\sigma^2} \Re \left\{ \sum_{m,n,k} \left[\frac{\partial y_{m,n,k}}{\partial \Theta_i} \right]^* \left[\frac{\partial y_{m,n,k}}{\partial \Theta_j} \right] \right\} \quad (5)$$

where $y_{m,n,k}$ is the noise-free version of $r_{m,n,k}$ in (4). Thus we have a 2×2 FIM in the form

$$\mathbf{J} = \begin{bmatrix} J_{v_r v_r} & J_{v_r v_t} \\ J_{v_t v_r} & J_{v_t v_t} \end{bmatrix} \quad (6)$$

with $J_{v_r v_t} = J_{v_t v_r}$, and the corresponding CRLBs on the radial and transverse velocities are given by, respectively,

$$\text{CRLB}^{(v_r)} = \frac{1}{\det \mathbf{J}} J_{v_t v_t}, \quad \text{CRLB}^{(v_t)} = \frac{1}{\det \mathbf{J}} J_{v_r v_r} \quad (7)$$

where $\det \mathbf{J} = J_{v_r v_r} J_{v_t v_t} - J_{v_r v_t}^2$.

According to the geometry of Fig. 1, we can project the radial and transverse velocity components along the direction \mathbf{e}_k by obtaining the projections v_{rk} and v_{tk} , respectively. It holds

$$v_k = v_{rk} + v_{tk} \quad (8)$$

where v_k is the projection of the velocity \mathbf{v} along the direction \mathbf{e}_k . Then, we can write

$$v_{n,k} = \frac{f_n}{c} (v_r + v_k). \quad (9)$$

The projections v_{rk} and v_{tk} can be obtained as [10]

$$v_{rk} = q_k v_r \quad (10)$$

$$v_{tk} = p_k v_t \quad (11)$$

where

$$q_k = \frac{d - x_k \sin \theta}{d_k} = \frac{1 - \frac{x_k \sin \theta}{d}}{\sqrt{1 + \frac{x_k^2}{d^2} - \frac{2x_k \sin \theta}{d}}} \quad (12)$$

$$p_k = \frac{x_k \cos \theta}{d_k} = \frac{x_k \cos \theta}{d \sqrt{1 + \frac{x_k^2}{d^2} - \frac{2x_k \sin \theta}{d}}}. \quad (13)$$

By substituting (10) and (11) in (8), and considering (9) in the model (4), we can compute the derivatives in (5) and obtain the components of the FIM

$$J_{v_r v_r} = \sum_n I_n \sum_k (1 + q_k)^2 \quad (14)$$

$$J_{v_t v_t} = \sum_n I_n \sum_k p_k^2 \quad (15)$$

$$J_{v_t v_r} = \sum_n I_n \sum_k p_k (1 + q_k) \quad (16)$$

where

$$I_n = \frac{2\pi^2 f_n^2 M \text{SNR} (M^2 - 1) T_{\text{sym}}^2}{3c^2} \quad (17)$$

and we defined the signal-to-noise ratio (SNR) as $\text{SNR} = P\beta^2/\sigma^2$. As it will be evident in the numerical results, for practical configurations in terms of antenna size, it holds $J_{v_r v_r} J_{v_t v_t} \gg J_{v_t v_r}^2$ so that $\det \mathbf{J} \approx J_{v_r v_r} J_{v_t v_t}$ and we have $\text{CRLB}^{(v_r)} \approx 1/J_{v_r v_r}$ and $\text{CRLB}^{(v_t)} \approx 1/J_{v_t v_t}$.

The limit for $d \rightarrow \infty$ in (12) is $q_k \rightarrow 1$ so that the right-hand summation in (14) tends to $4K$. Thus, for the estimation of the radial velocity component v_r , the information (14) tends to the inverse of the traditional CRLB for velocity estimation in far-field conditions, which is given by [15]

$$\text{CRLB}^{(v_r)} = \frac{3c^2}{8\pi^2 f_c^2 MNK \text{SNR} (M^2 - 1) T_{\text{sym}}^2} \quad (18)$$

where we considered $f_n \approx f_c$ since $B \ll f_c$. Notice that $(M^2 - 1)T_{\text{sym}}^2$ is approximately the squared signal duration T_{obs}^2 , and in (18) it is highlighted the SNR gain MNK obtained thanks to the exploitation of M symbols, N subcarriers and K antennas for the estimation. When $\theta = 0$, (14) becomes

$$J_{v_r v_r} = \frac{2\pi^2 f_c^2 M N \text{SNR} (M^2 - 1) T_{\text{sym}}^2}{3c^2} \sum_k \left(1 + \frac{1}{\sqrt{1 + k^2 \frac{\delta^2}{d^2}}} \right)^2 \quad (19)$$

Interestingly, the information on the target's radial velocity reduces as the distance d from the array decreases, since $k^2 \delta^2 / d^2 > 0$, resulting in an SNR gain lower than K for a small distance. However, for practical array dimensions and operating distances (in particular, when the distance becomes significantly higher than the largest x_k , i.e., than the array aperture $D_{\text{elaa}} = (K - 1)\delta$), the term $k^2 \delta^2 / d^2$ is small. Therefore, as far as the distance d exceeds the array aperture D_{elaa} , we have $1/J_{v_r v_r} \rightarrow \text{CRLB}^{(v_r)}$ in (18) which does not depend on the distance d and on the array aperture D_{elaa} .

For what concerns the transverse velocity, its estimation at a large distance is not possible; in fact, we have $p_k \rightarrow 0$ for $d \rightarrow \infty$ (in practice, when d is much larger than the array aperture D_{elaa}) so that $J_{v_t v_t} \rightarrow 0$ and no information can be retrieved. Differently, when the array aperture increases and/or the distance decreases, we have $p_k \neq 0$, and transverse velocity estimation becomes feasible. The information on transverse velocity is maximum on the boresight direction of the ELAA according to (15) and (13) (i.e., $\theta = 0$); differently, it is not possible to estimate the transverse velocity when $\theta = \pm \frac{\pi}{2}$. In fact, in this case, the direction \mathbf{e}_k is the same for all the antennas and corresponds to the radial direction, so no further information becomes available rather than the radial velocity. The same behavior is experienced in near-field distance estimation with uniform linear arrays (ULAs), which is not possible for $\theta = \pm \frac{\pi}{2}$ [16]. For the case of transverse velocity estimation, we can write for $\theta = 0$

$$J_{v_t v_t} = \frac{2\pi^2 f_c^2 M N \text{SNR} (M^2 - 1) T_{\text{sym}}^2 \delta^2}{3c^2 d^2} \sum_k \frac{k^2}{1 + k^2 \frac{\delta^2}{d^2}} \quad (20)$$

which decreases with the square of the distance d . Considering the practical case where the target is not very close to the BS, the term $k^2 \delta^2 / d^2$ is generally small, and the following approximate expression is obtained

$$\begin{aligned} J_{v_t v_t} &\approx \frac{\pi^2 f_c^2 M N K \text{SNR} (M^2 - 1) T_{\text{sym}}^2 (K^2 - 1) \delta^2}{18c^2 d^2} \\ &\approx \frac{\pi^2 f_c^2 M N K \text{SNR} T_{\text{obs}}^2 D_{\text{elaa}}^2}{18c^2 d^2}. \end{aligned} \quad (21)$$

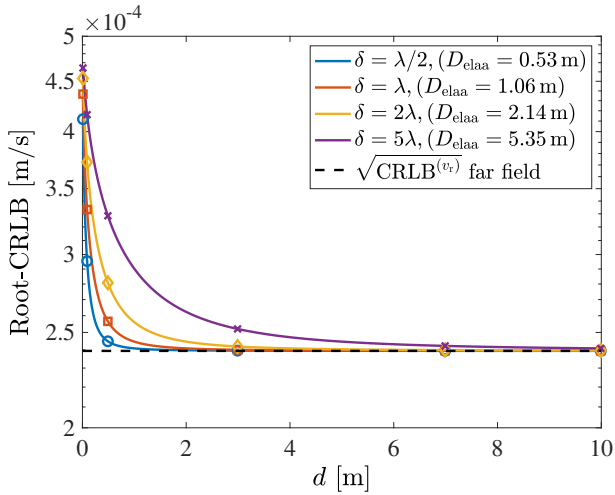


Fig. 2. Root-CRLB for the radial velocity as a function of the distance d for different apertures D_{elaa} . Markers stand for $\sqrt{1/J_{v_r v_r}}$ in the same setting.

As for the traditional CRLB on radar-based velocity estimation in (18), the information on the transverse velocity is proportional to the squared signal duration. Larger carrier frequency f_c is beneficial for both radial and transverse velocity estimation. The adoption of a proper array aperture D_{elaa} can be traded to achieve the required transverse velocity accuracy depending on the operating distance d , while the SNR and the symbol time have the same impact on both the components.

Expression (21) shows a deep difference between what happens in the near field for distance estimation and transverse velocity estimation. In fact, in near-field distance estimation, the CRLB is proportional to $d^2/f_c^2 D_{\text{elaa}}^4$ [16]; as a result, in that case, the root-CRLB is inversely proportional to the Fraunhofer distance $d_{\text{ff}} = 2D_{\text{elaa}}^2/\lambda$, with $\lambda = c/f_c$. Therefore, increasing the array aperture D_{elaa} (i.e., number of antennas, antenna spacing) and/or the carrier frequency is beneficial for the estimation quality, with a larger impact of the array aperture. Instead, in transversal velocity estimation using ELAAs, the parameters affecting the quality are the same according to (21), but they influence the bound all with the second power. Differences are evident when considering a half-wavelength spaced array ($\delta = \lambda/2$). In this case, the information on the transverse velocity is

$$J_{v_t v_t} \approx \frac{\pi^2 M N K \text{SNR} (M^2 - 1) T_{\text{sym}}^2 (K^2 - 1)}{72d^2} \quad (22)$$

which does not depend on the carrier frequency, differently from the radial velocity estimation or what happens for near-field distance estimation. These results suggest that the possibility of gathering information on the transverse velocity is not strictly related to the near-field behavior intended as spherical wavefront propagation, rather than on the geometrical aspects enabling to project the target velocity along the set of directions corresponding to the different antennas of the array.

IV. NUMERICAL RESULTS

We now present some results concerning the quality of velocity estimation using a linear ELAA. If not differently

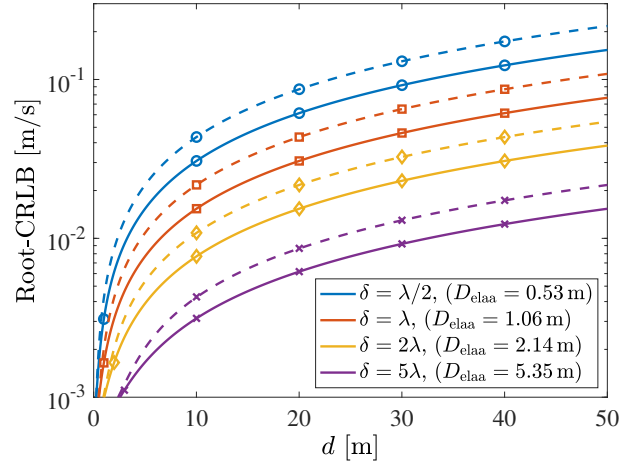


Fig. 3. Root-CRLB for the transverse velocity as a function of the distance d for different apertures D_{elaa} . Continuous lines (—) are for $\theta = 0^\circ$; dashed lines (- -) are for $\theta = 45^\circ$. Markers stand for $\sqrt{1/J_{v_t v_t}}$ in the same setting.

specified, we consider $f_c = 28$ GHz, $K = 101$ antennas, $N = 1$ and $\text{SNR} = 0$ dB. A packet with $M = 14$ OFDM symbols is considered, and symbol time $T_{\text{sym}} = 16.6$ ms. According to the expressions reported in Sec. III, the presented root-CRLB curves will scale with \sqrt{N} when considering $N > 1$.

Fig. 2 shows the root-CRLB for the radial velocity estimation in (7)-left as a function of the distance d , for a small distance from the array. Markers indicate the approximation obtained as $\sqrt{1/J_{v_r v_r}}$, with $J_{v_r v_r}$ given by (19), showing that it is very tight for the condition of interest. The traditional far-field CRLB according to (18) is reported for comparison. Results are given for different apertures D_{elaa} , but with the same number of antennas K in order to consider a constant overall received power. As it is possible to notice, a small deviation from the far-field CRLB is experienced only at very small distance from the array, in particular, for a distance below the array aperture D_{elaa} , region also known as *geometric near field* [11].

In Fig. 3 the root-CRLB for the transverse velocity in (7)-right is reported as a function of the distance d , considering $\theta = 0$ and $\theta = 45^\circ$. Again, the comparison between the exact root-CRLB and its approximation $\sqrt{1/J_{v_t v_t}}$ (markers) shows a very good agreement. It can be noticed that the accuracy decreases as the distance d increases, as well as when the angle increases. The array aperture D_{elaa} has a fundamental role in achieving a good estimation quality.

Fig. 4 compares accuracy related to the radial velocity (blue curves with \square) and to the transverse velocity (red curves with $+$) in terms of root-CRLB as a function of the distance d for a fixed number of antennas K , a half-wavelength antenna spacing $\delta = \lambda/2$ and two different carrier frequencies, i.e., $f_c = 28$ GHz (continuous lines) and $f_c = 6$ GHz (dashed lines). Thus, the two conditions translate in two different array apertures D_{elaa} . It is possible to notice that the radial accuracy is close to the traditional CRLB (yellow curves with \circ), and it is always larger than the transverse one. In fact, by comparing

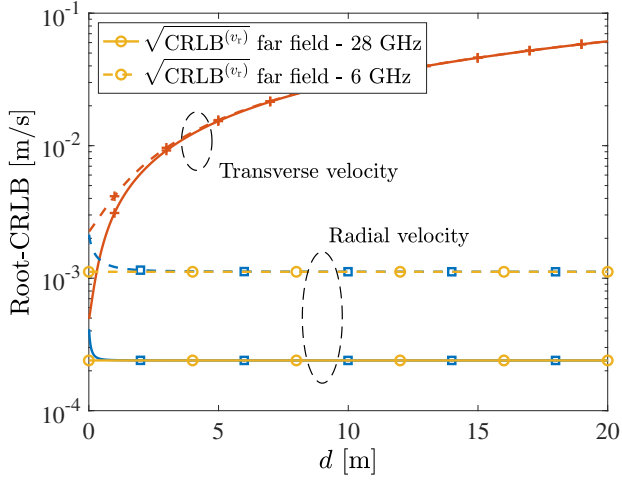


Fig. 4. Root-CRLB for radial (\square) and transverse ($+$) velocities as a function of the distance d for different carrier frequencies and $\delta = \lambda/2$ (angle $\theta = 0$). Continuous lines (—) are for $f_c = 28$ GHz; dashed lines (---) are for $f_c = 6$ GHz. Comparison with the far-field CRLB in (18).

(18) and (21) it can be seen that when $d = D_{\text{elaa}}/(4\sqrt{3})$, the estimation quality for the radial velocity equals the estimation quality for the transverse one, at $\theta = 0$. Thus, an operating distance smaller than the array aperture D_{elaa} is required to achieve a balance in terms of estimation quality among the different components of the velocity. Moreover, the radial velocity accuracy slightly deteriorates when close to the array. The transversal velocity accuracy does not depend on the carrier frequency, since we are comparing the results considering half-wavelength antenna spacing; differently, the estimation quality for the radial velocity improves as the carrier frequency increases.

Finally, a 2D map considering the distribution of the root-CRLB for the transverse velocity in the semi-plane in front of the ELAA is reported in Fig. 5. In this case, we considered a transmit power $P_T = 23$ dBm and a receiver noise figure $F = 9$ dB, to include the impact of the path loss in the SNR. A target with radar cross section of 1 m^2 is assumed, and 0 dBi gain antennas. As evident, the transversal accuracy decreases as the distance from the array increases due to the combined effect of the term d^2 in (21) and of the SNR scaling; moreover, it deteriorates at large angles, due to the use of the linear array.

V. CONCLUSION

This paper laid the foundation for estimating radial and transverse velocity components of a moving target using a linear ELAA, by analytically deriving the corresponding CRLBs. The results show that the accuracy of transverse velocity estimation decreases with the square of the target-antenna distance, and it is unaffected by the carrier frequency when using a half-wavelength spaced array. This behavior contrasts with the radial velocity component and also differs from near-field distance estimation. These findings suggest that transverse velocity estimation is not strictly tied to the wavefront sphericity typical of the near field, but rather depends on the geometrical arrangement of the array relative to the

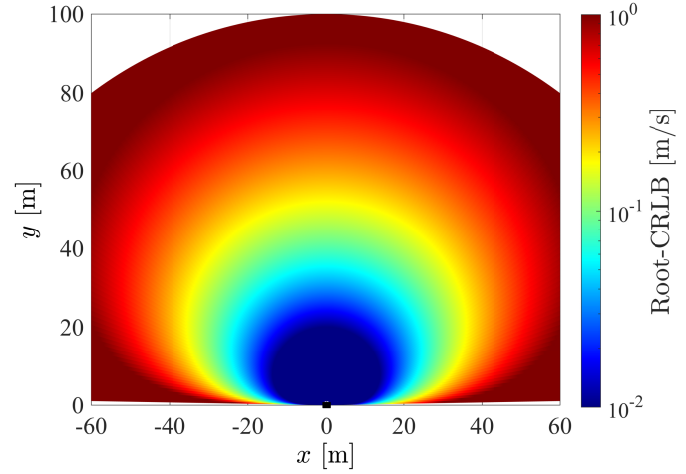


Fig. 5. Distribution of the root-CRLB for transverse velocity on the 2D plane.

target's position. Hence, the array aperture plays a crucial role in achieving a satisfactory performance.

REFERENCES

- [1] F. Liu *et al.*, "Integrated sensing and communications: Toward dual-functional wireless networks for 6G and beyond," *IEEE J. Select. Areas Commun.*, vol. 40, no. 6, pp. 1728–1767, Mar. 2022.
- [2] S. J. Orfanidis, *Electromagnetic Waves and Antennas*. New Jersey, USA: Rutgers University, 2008.
- [3] D. Dardari and N. Decarli, "Holographic communication using intelligent surfaces," *IEEE Commun. Mag.*, vol. 59, no. 6, pp. 35–41, June 2021.
- [4] M. Cui *et al.*, "Near-field MIMO communications for 6G: Fundamentals, challenges, potentials, and future directions," *IEEE Commun. Mag.*, vol. 61, no. 1, pp. 40–46, Jan. 2023.
- [5] Z. Wang *et al.*, "A tutorial on extremely large-scale MIMO for 6G: Fundamentals, signal processing, and applications," *IEEE Communications Surveys & Tutorials*, pp. 1–1, 2024, early access.
- [6] A. Sakhnini *et al.*, "Near-field coherent radar sensing using a massive MIMO communication testbed," *IEEE Trans. Wireless Commun.*, vol. 21, no. 8, pp. 6256–6270, Aug. 2022.
- [7] S. K. Dehkordi *et al.*, "Multi-static parameter estimation in the near/far field beam space for integrated sensing and communication applications," *arXiv e-prints*, 2023.
- [8] Z. Wang, X. Mu, and Y. Liu, "Near-field integrated sensing and communications," *IEEE Commun. Lett.*, vol. 27, no. 8, pp. 2048–2052, Aug. 2023.
- [9] Q. He, R. S. Blum, H. Godrich, and A. M. Haimovich, "Cramer-Rao bound for target velocity estimation in MIMO radar with widely separated antennas," in *2008 42nd Annual Conference on Information Sciences and Systems*, 2008, pp. 123–127.
- [10] Z. Wang, X. Mu, and Y. Liu, "Near-field velocity sensing and predictive beamforming," *arXiv e-prints*, 2024.
- [11] N. Decarli and D. Dardari, "Communication modes with large intelligent surfaces in the near field," *IEEE Access*, vol. 9, pp. 165 648–165 666, Dec. 2021.
- [12] A. Guerra, F. Guidi, D. Dardari, and P. M. Djuric, "Near-field tracking with large antenna arrays: Fundamental limits and practical algorithms," *IEEE Trans. Signal Processing*, vol. 69, pp. 5723–5738, Aug. 2021.
- [13] H. Chen *et al.*, "6G localization and sensing in the near field: Features, opportunities, and challenges," *arXiv e-prints*, 2023.
- [14] S. M. Kay, *Fundamentals of Statistical Signal Processing: Estimation Theory*. Upper Saddle River, NJ: Prentice-Hall, 1993.
- [15] M. Braun, "OFDM radar algorithms in mobile communication networks," *Karlsruher Institutes für Technologie*, 2014.
- [16] M. N. E. Korso, R. Boyer, A. Renaux, and S. Marcos, "Conditional and unconditional Cramér-Rao Bounds for near-field source localization," *IEEE Trans. Signal Processing*, vol. 58, no. 5, pp. 2901–2907, May 2010.